



A four-element fractional creep model of weakly cemented soft rock

Jiashun Liu^{1,2} · Hongwen Jing² · Bo Meng² · Laigui Wang³ · Jianjun Yang¹ · Xuefeng Zhang¹

Received: 24 November 2019 / Accepted: 27 May 2020 / Published online: 13 July 2020
© Springer-Verlag GmbH Germany, part of Springer Nature 2020

Abstract

The creep model is the main form used to describe the creep behavior of weakly cemented soft rock (WCSR). To investigate the creep behavior of weakly cemented soft rock, multi-stage loading creep tests were performed by using GDS HPTAS creep triaxial apparatus. The creep curves, creep rates, and creep failure modes of weakly cemented soft rock under different water contents were obtained. A novel four-element fractional-order creep model to describe the three-stage creep behavior of weakly cemented soft rock was proposed using the Abel dashpot basing on the creep test results and fractional calculus theory. The formula of this model was developed according to the H-Fox special function. The trust-region method was used to obtain the model parameters, and the parameters were optimized using the ant colony optimization approach. The creep curves of weakly cemented soft rock under different water contents were calculated and compared with the experimental results, verifying the superiority of the four-element fractional-order creep model in describing the creep characteristics of weakly cemented soft rock. The calculated results were also in good agreement with the experimental results, which confirms that the four-element fractional order creep model can accurately reflect the complete creep behavior of weakly cemented soft rock.

Keywords Weakly cemented soft rock · Fractional-order calculus · Four-element fractional order creep model · GDS creep triaxial apparatus · Creep curve

Abbreviations

w	Water content	ρ	Density
Γ	Gamma function	δ	Pheromone volatilization
I	Integral symbols	D	Differential symbols
α	Fractional order	ξ, ξ_1, ξ_2	Viscosity coefficient of the Abel dashpot
σ_s	Stress threshold	E_0, E_1	Elastic moduli of the Hooke body
σ_1	Stress of the Hooke body	η_1, η_2	Viscosity coefficients of the Newton body
σ_2	Stress of the Abel dashpot	ε_1	Strain of the Hooke body
σ_3	Stress of the plastic	ε_2	Strain of the Abel dashpot
σ_c	Uniaxial compressive strength	ε_3	Strain of the plastic element
ε_a	Axial strain	σ_0	Deviator stress
Δt (Tomanovic)	Error of the creep model	ε_r	Radial strain
		β	Basic parameter

✉ Jiashun Liu
liujiashun000@163.com

¹ College of Civil Engineering, Liaoning Technical University, Fuxin 123000, Liaoning, People's Republic of China

² State Key Laboratory for Geomechanics and Deep Underground Engineering, China University of Mining & Technology, Xuzhou 221116, Jiangsu, People's Republic of China

³ School of Mechanics and Engineering, Liaoning Technical University, Fuxin 123000, Liaoning, People's Republic of China

Introduction

Many engineering problems, such as the uneven settlement of foundations, the deformation of underground structures, and casing damage, are caused by the strong creep behavior of weakly cemented soft rock (WCSR) (Xu and Chen 2013; Xu and Jiang 2017). The weakly cemented soft rock shows significant rheological characteristics under long-term loading and exposure to water (Roedder and Bassett 1981; Sun and Wang 2000). The physicochemical interaction between water

and rock not only reduces the friction angle and cohesion of WCSR but alters the mineral composition and microstructure of the rock, thereby aggravating crack initiation and propagation (Jiang et al. 2014; Matthess 1988). These changes lead to deterioration of the strength and rigidity of WCSR, which can result in engineering disasters.

The effect of the water content on the mechanical properties of rock is a particularly prominent topic among researchers. Chenevert (1970) studied the decrease in strength experienced by mudstone through water absorption; Ajalloeian and Lashkaripour (2000) utilized the exponential relationship between mudstone strength and water content to predict the uniaxial compressive strength at different water contents. Işık (2010) concluded that even a very small increase in the water content can cause considerable loss of the uniaxial compressive strength of gypsum. Shi et al. (2016) studied rock strength data at various water contents and demonstrated that sand-stone strength and water content have a negative exponential relationship. In addition, research has also shown that the water content has a significant effect on the creep behavior of rock (Hong et al. 2015; Wei et al. 2018). A series of shear creep tests on the weak structural plane of sandstone at different water contents has also been conducted (Li et al. 2008). Huang and Liu (2011) studied the effect of changes in the moisture content on the creep properties of siltite and proposed a mathematical relationship between the creep modulus and moisture content. Liu et al. (2015) analyzed the creep properties of rock with different moisture contents and the relationship between the moisture content and creep mechanical properties. The research results showed that the ratio of the creep strain and instantaneous strain, the initial, steady, and ultimate accelerated creep rates increased, while the long-term strength of the red bed mudstone decreased with an increase in the water content (Ju et al. 2016). The creep test result of loess show that the creep strain increases with an increase of moisture content and decreases with an increase in confining pressure (Tang et al. 2020). In general, water content and stress are important factors affecting rock creep characteristics (Deng et al. 2016; Feng et al. 2020; Yang et al. 2007; Zhang et al. 2013). Therefore, it is necessary to consider the effect of the water content conditions on the creep behavior of weakly cemented soft rock.

Creep behavior is one of the most important mechanical properties of rock, and creep modeling is the main characterization technique for this property (Duan et al. 2013; Hou et al. 2019; Li et al. 2013; Wu et al. 2014, 2015). Thus, to establish a reasonable creep model, a quantitative description of the influence of creep effects, strain rate, and stress relaxation on the strength and deformation characteristics of WCSR is necessary. In recent decades, numerous creep models have been proposed to simulate the behavior of rock creep (e.g., the Maxwell, Kelvin, and Nishihara models) (Chen et al. 2015; Ofoegbu et al. 2017; Tomanovic 2006). At present, creep constitutive models for WCSR mainly include empirical models, element

models, and the viscoelastic–plastic mechanical model (Zhou et al. 2011, 2013; Liao et al. 2016; Liu et al. 2016; Metzler and Nonnenmacher 2003). As such, the element combination models, which have strong theoretical properties, a strict mechanics deduction process, and parameters with clear physical meaning, have been widely employed to study the creep characteristics of geotechnical materials. However, accelerated creep has not yet been well described by the integral order component model. Fractional calculus theory can be employed to study the differential of any order and can describe the creep behavior of geotechnical materials in addition to the evolution of structural characteristics (Arikoglu 2014; Heymans and Bauwens 1994; Papoulia et al. 2010; Pu et al. 2018). Fractional calculus has been considered as one of the best tools for modeling the physical responses of materials owing to its flexibility. Moreover, many creep models have been established. For example, Yuan (2014) proposed a creep model to describe the creep damage characteristics of mudstone using fractional calculus theory, while Tang et al. (2017) proposed a new four-element rock creep model based on the variable-order fractional derivative and continuum damage mechanics. In addition, Chen et al. (2014) proposed a fractional-order theological model to describe the creep behavior of fractured mudstone based on the fractional calculus and three-parameter theological models, while Li established a fractional derivative of the Burgers model based on strain energy theory, where the model parameters were obtained using the particle swarm optimization method (Li et al. 2018). Furthermore, Zhang established a new three-element nonlinear stress relaxation model for Nanning expansive soils based on fractional calculus theory (Zhang et al. 2014).

However, despite the recent improvements in creep models of geotechnical materials, the majority of universal models cannot fully describe the accelerated creep characteristics of soft rock, and the relationship between creep properties and experimental conditions remains unclear (Bouras et al. 2018; Xu and Jiang 2017; Zhou et al. 2013). Thus, we herein report our study involving multi-stage loading creep tests of weakly cemented soft rock under different water content conditions. A novel four-element fractional-order creep model was developed using the Abel dashpot instead of the Kelvin clay pot element, in addition to taking the plastic element instead of the elastic element. The model parameters of the four-element creep model were obtained using the trust-region method. Finally, the reliability of the four-element model was verified.

Creep tests and results analysis

Rock samples

The rock samples employed in the multi-stage loading creep tests were taken from the Jurassic mudstone strata in the main

inclined shaft of the Hongqingliang Coal Mine, in Erdos City, Inner Mongolia. The rock sample density (ρ) was 2.41 g/cm³, and the natural water content (w) was 7.9%.

X-Ray diffraction measurements showed that the mineral composition of the rock samples was as follows: quartz, 31.6%; montmorillonite, 18.9%; albite, 15.9%; illite, 15.4%; and kaolinite, 18.2%. It should be noted that the hydrophilic viscous minerals present in the rock (i.e., montmorillonite, illite, and kaolinite) are responsible for the facile disintegration of soft rock in water. This rock adopts a block structure exhibiting porosity cementation and belongs to the group of medium expansive WCSR.

The rock was prepared in cylindrical samples, which diameter (φ) is 50 mm and height (h) is 100 mm, using a YBZS-100 rock coring machine and cutting apparatus according to test procedures reported by the ISRCSC. Four groups of WCSR samples with water contents of 0% (dry state), 7.9% (natural state), 14.5%, and 21.6% (saturated state) were prepared using drying and natural immersion methods, as appropriate. The processed samples exhibited good integrity.

Creep test scheme

The multi-stage loading creep tests of the WCSR samples were performed using the GDS HPTAS creep triaxial apparatus, which is shown in Fig. 1. The axial loaded value of the apparatus can reach 250 kN, and its lowest loading rate is 0.01 mm/min. This apparatus can be employed for stress or strain control tests.

The uniaxial compressive strength (σ_c) obtained from the uniaxial compression test was used as the loading basis for the creep tests, where the confining pressure was 6 MPa, and the maximum loading stress was about 0.7 σ_c times the uniaxial strength.

The majority of the creep tests performed showed that the geotechnical materials exhibited a memory effect for the

loading history. According to the principle of linear superposition, the creep curves of WCSR under different stress levels and water contents can be obtained. Therefore, multi-stage loading creep tests of the WCSR were performed. The creep experiment was divided into three stages: (1) The advanced loading module was used to apply the confining pressure and axial pressure at a loading rate of 0.05 MPa/s until a pressure of 6 MPa was reached, which was a preset value set according to the actual working environment of weakly cement soft rock. The specimen was in an initial isotropic stress state after confining pressure loading (Su et al. 2019). (2) A loading rate of 0.1 MPa/s was then employed until the deviator stress reached the predicted value while the confining pressure was kept constant. (3) Multi-stage loading creep tests of the WCSR were performed and a loading time of 50 h was employed for each stage. When the creep rate became less than or equal to 0.01 mm/min (i.e., a stable creep stage), the subsequent level of load was stopped. The test was stopped when the deformation rate exceeded 0.05%·h⁻¹ of the accelerated creep stage. All of the creep test data were recorded during the test and the multi-stage loading scheme are outlined in Table 1.

Analysis of creep test results

Creep deformation

The soft rock samples were found to exhibit obvious creep behavior characteristics during the various creep tests, but no significant brittle failure was observed. The results of the axial strain and radial strain under different deviator stresses and water contents were obtained, as shown in Fig. 2.

The results show that the deformation of WCSR increases with the load time. The total deformation includes instantaneous deformation and creep deformation. However, the creep curves present in different forms with different water content and deviator stress. More specifically, attenuation creep and constant rate creep behavior were observed when the deviator stress (σ_0) was relatively small, and accelerated creep behavior occurred only for larger deviator stress (σ_0) values. In addition, the creep curves of WCSR indicate typical creep characteristics, including attenuation creep, constant rate creep, and accelerated creep. An increase in the deviator stress leads to



Fig. 1 Triaxial rheometer apparatus (GDS HPTAS)

Table 1 Multi-stage loading scheme employed for the rheology tests

Water contents w (%)	Deviator stress (MPa)
0.0	5.0, 8.0, 11.0, 13.0, 14.5
7.9	3.0, 5.0, 7.0, 9.0, 10.5
14.5	2.0, 4.0, 6.0, 8.0
21.6	2.0, 4.0, 6.0

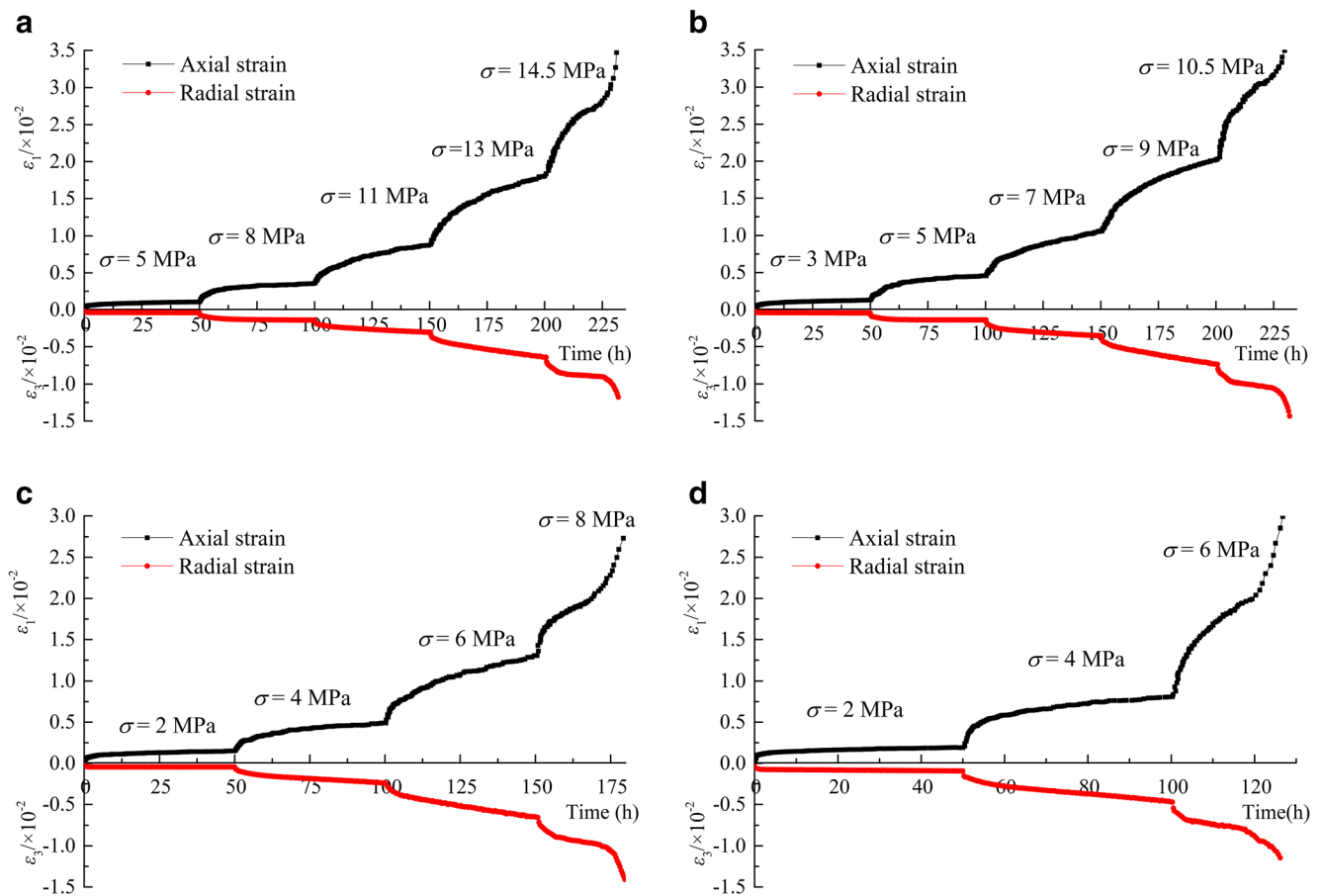


Fig. 2 Creep test results. (a) $w = 0\%$; (b) $w = 7.9\%$; (c) $w = 14.5\%$; (d) $w = 21.6\%$

damage and destruction of the internal structure of the soft rock specimen, thereby increasing the creep deformation. A higher deviator stress will lead to the rock sample reaching a steady state or accelerated state more rapidly.

Figure 2 also shows that accelerated creep behavior occurs when the water content (w) is 0% and the deviator stress (σ_0) is 14.5 MPa. More specifically, We also note that the deviator stress (σ_0) which correspond to the occurrence of accelerated creep were 10.5, 8.0, and 6.0 MPa when the water content was 7.9%, 14.5%, and 21.6%, respectively. Therefore, the water content has a significant effect on the creep behavior of WCSR. This occurs mainly due to the presence of expansive minerals, such as montmorillonite, illite, and kaolinite, which expand through water absorption with increasing water content. This also reduces the bonding structure potential between particles and increases the damage to the rock mass. Furthermore, the lubrication caused by the water film leads to a decrease in the internal friction structure potential of the rock, which in turn reduces the friction strength between the rock structures and causes a transition from steady-state creep to unsteady creep, until accelerated creep occurs.

The radial creep curves were found to be similar to the axial creep curves. More specifically, the radial creep was negative due to the lateral expansion deformation of the soft rock

specimen. In addition, the radial creep deformation was significantly smaller than the axial creep deformation because the confining pressure effectively limited the lateral deformation.

Creep rate

The creep rate is an important index that reflects the behavior of creep curves. The creep rate can be obtained according to the first derivation of the creep test results, as shown in Fig. 3.

Figure 3 shows that the creep rate curve shows two forms. More specifically, each steady-state creep rate curves include a steeply descending stage and stationary holding stage, while except these two stages, each unsteady creep rate curves also include the sharply increasing stage. However, the creep rate curves fluctuate to some extent due to the differences between samples caused by the inhomogeneity of the geomaterial components.

The initial creep rate and steady creep rate are important for the creep properties of weakly cement soft rock. Therefore, the initial creep rate and steady creep rate under different water content conditions can be obtained according to creep rate curves of Fig. 3, as shown in Fig. 4.

Figure 4 shows that the creep rate is significantly affected by water content and deviator stress. Figure 4a shows that the

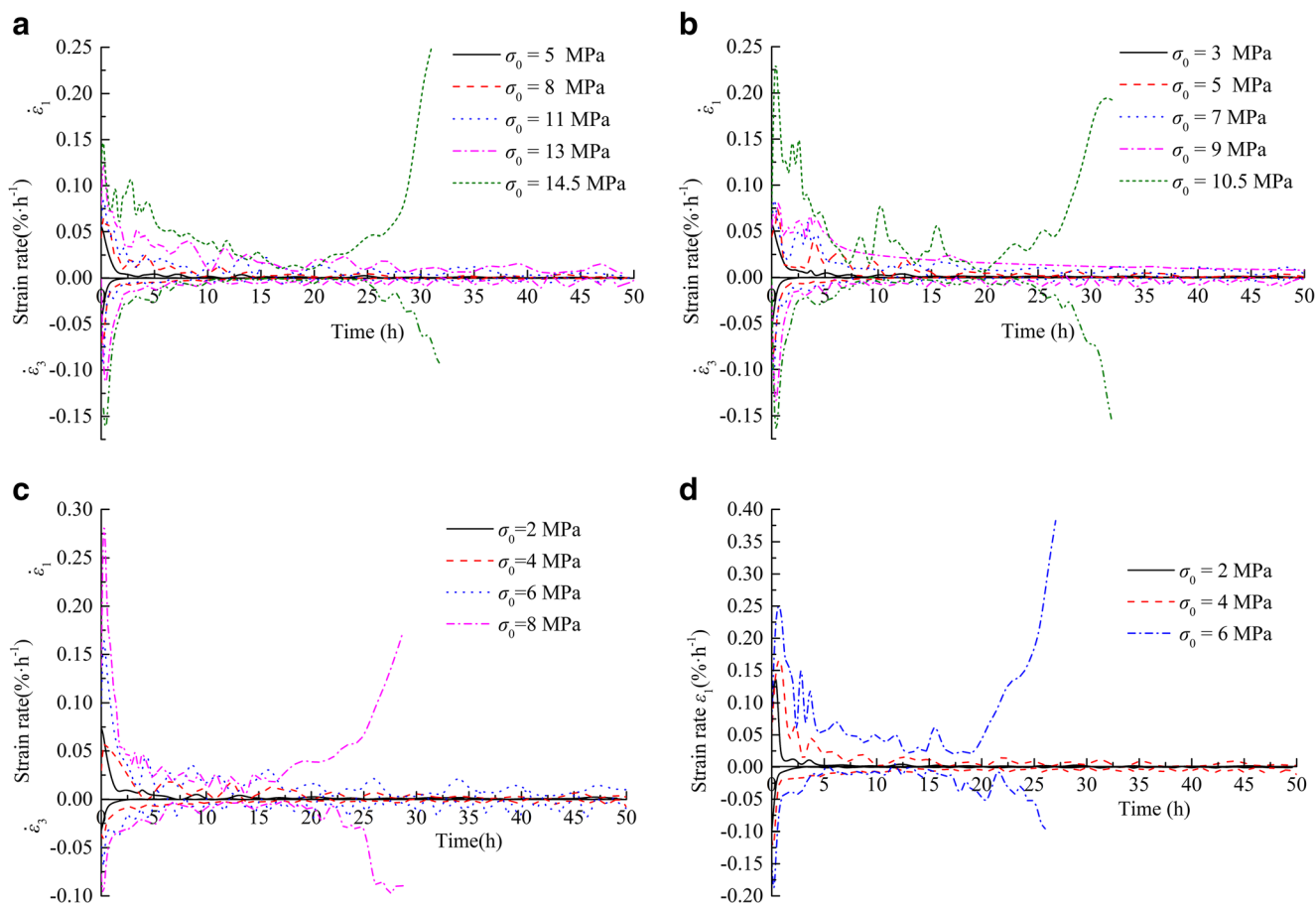


Fig. 3 Creep rate curves. (a) $w = 0\%$; (b) $w = 7.9\%$; (c) $w = 14.5\%$; (d) $w = 21.6\%$

axial initial creep rate increases with deviator stress and water content increase. However, influence of water content on the radial initial creep rate curves is not consistent. For example, when water content is 14.5%, the radial initial creep rate is 0.0325, 0.0445, 0.0695, and 0.11125%·h⁻¹, corresponding to deviator stress is 2, 4, 6, and 8 MPa of water, respectively.

Nevertheless, when water content is 7.9%, the radial initial creep rate is 0.05438, 0.09493, 0.11152, 0.14793, and 0.18435%·h⁻¹, corresponding to deviator stress is 3, 5, 7, 9 and 10.5 MPa, respectively. This indicates that the radial initial creep rate of water content (7.9%) is larger than that of water content (14.5%). In addition, the other experimental

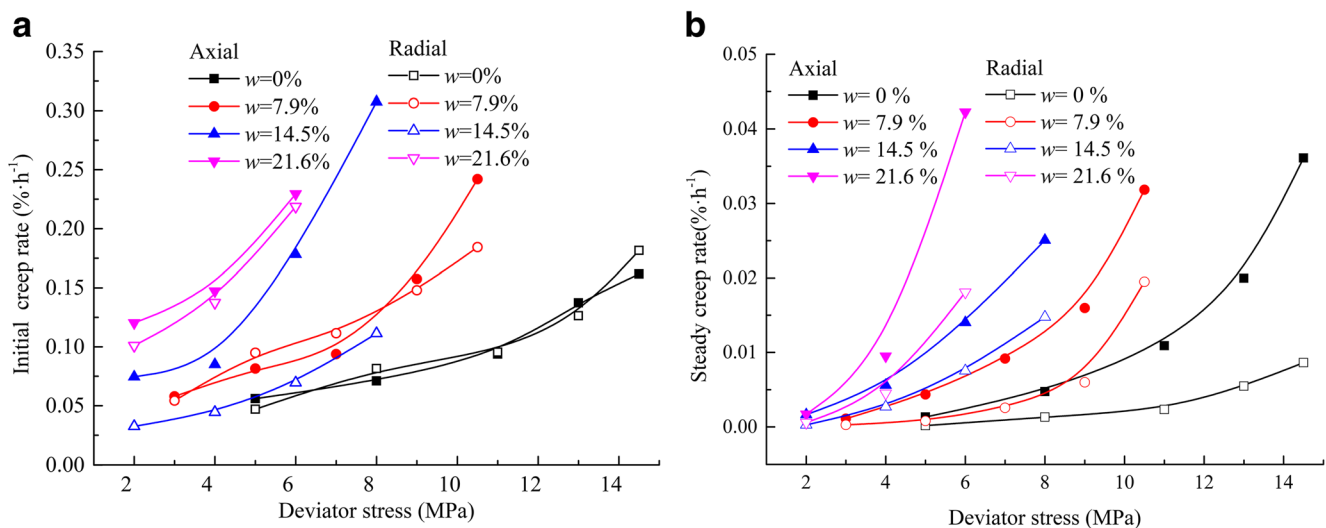


Fig. 4 Creep rate curves: (a) initial creep rate, (b) steady creep rate

results are consistent with the viewpoint that the initial creep rate increases with the increase of water content and deviator stress.

We also note that the axial initial creep rate is larger than radial initial creep rate when water content is larger than 14.5%. At the same time, the axial initial creep rate is considerably close to the radial initial creep rate when water content is smaller than 7.9% (natural water content). This can be explained as that the internal structure of rock mass is softened and the strength is weakened seriously with higher water content, while the radial initial creep rate is restrained by confining pressure in the initial stage.

Figure 4b shows that the steady creep rate increases with water content and deviator stress increase, which indicates that a higher water content and deviator stress will enhance the occurrence of creep deformation. The axial steady creep rate is always larger than the radial steady creep rate. The axial steady creep rate ranges from $0.00132\% \cdot \text{h}^{-1}$ to $0.04227\% \cdot \text{h}^{-1}$ and the radial steady creep rate ranges from $0.00017\% \cdot \text{h}^{-1}$ to $0.0181\% \cdot \text{h}^{-1}$. This indicates that the axial creep deformation is more intense than the radial creep deformation. The failure mode of the weakly cemented soft rock specimen had also been shown to be dominated by longitudinal crack generation, expansion, and penetration. Therefore, it is necessary to pay particular attention to the creep deformation corresponding to the direction of the major principal stress to avoid deformation failure as part of the long-term stability evaluation process of underground engineering.

Instantaneous deformation and creep deformation

The creep test curves of the WCSR include instantaneous deformation and creep deformation. It should be noted that instantaneous deformation is an important index for the modulus characteristics of rock samples and the creep deformation is mainly employed to measure the long-term stability of underground engineering surrounding rock. The initial deformation values, which were obtained at the time when the deviator stress was just constant, were taken as the instantaneous deformation. The creep deformation was obtained by differentiating the instantaneous deformation with respect to the total deformation at the end of the creep tests. The instantaneous deformation and the creep deformation under different water content and deviator stress conditions are shown in Table 2. The strain ratio in Table 2 refers to the ratio of the instantaneous strain to the creep strain of the WCSR under this level of load.

Table 2 shows that the instantaneous deformation and creep deformation increases with an increase in the deviator stress and water content. The ratio of the axial instantaneous deformation to the creep deformation is approximately 0.01–0.15, while the ratio of the radial deformation to the creep deformation is approximately 0.09–0.92. This indicates that the creep deformation of WCSR is dominant. The ratio is

larger when the deviator stress is lower and the creep curves indicate long-term steady creep. The ratio of the radial instantaneous deformation to the creep deformation is larger than that of the axial deformation. This result can be accounted for by the expansion deformation of WCSR specimens under the combined actions of an applied load and a specific water content. Moreover, as the degree of expansion deformation decreases gradually with time, more time is required to complete the expansion deformation process. This part of the deformation process plays an important role in the creep test; however, the expansion deformation of soft rock cannot be removed from the test data.

In addition, the ratio of the axial instantaneous deformation to the radial instantaneous deformation is approximately 0.35–1.11, while the creep ratio is approximately 1.94–5.54. This can be explained by the fact that instantaneous deformation occurred in the initial loading stage, radial expansion deformation occurred rapidly, and axial deformation was limited. In addition, the axial creep deformation increased with increasing loading time in the creep stage, but radial creep deformation was limited due to the confining pressure effect.

Long-term strength

Long-term strength is an important index for evaluating the long-term stability of underground engineering structures and estimating whether accelerated creep occurs. Stress–strain isochronous curves are the main method used to determine the long-term strength of rock. However, it is difficult to describe the regularity of the inflection point of stress–strain isochronous curves accurately, which results in a certain amount of uncertainty when determining the long-term strength. The operation of this method is also complex when there are many data. The reciprocal of the steady creep rate method was used to determine the long-term strength of weakly cemented soft rock in this study according to Wang et al. (2018). Two linear functions were used to fit the curve between the reciprocal of the steady creep rate and the deviator stress when the stress was high and low, respectively. The intersection of the two fit curves was taken as the long-term strength of the soft rock. The long-term strength results are shown in Fig. 5, where Fig. 5a was obtained by using the reciprocal of the axial steady creep rate and Fig. 5b was obtained by using the reciprocal of the radial steady creep rate.

Figure 5 shows that the long-term strength of the rock decreases with an increase of the water content. The long-term strengths of the rock were 8.402, 5.241, 4.381, and 4 MPa via the reciprocal of the axial steady creep rate, and 8.052, 5.614, 4.105, and 4 MPa via the reciprocal of the radial steady creep rate when the water content was 0%, 7.9%, 14.5%, and 21.6%, respectively. However, the long-term strength difference between the axial and radial creep rates is insignificant. Therefore, the average values were taken to describe the relationship between the long-term strength and

Table 2 Instantaneous strain and creep strain

Water content (%)	Deviator stress (MPa)	Axial strain			Radial strain		
		Instantaneous strain (%)	Creep strain (%)	Strain ratio	Instantaneous strain (%)	Creep strain (%)	Strain ratio
0	5	0.014	0.093	0.151	-0.017	-0.023	0.739
	8	0.017	0.237	0.072	-0.028	-0.073	0.384
	11	0.021	0.503	0.042	-0.034	-0.130	0.262
	13	0.029	0.921	0.031	-0.044	-0.294	0.15
	14.5	0.043	1.594	0.027	-0.061	-0.474	0.129
7.9	3	0.014	0.113	0.124	-0.020	-0.026	0.769
	5	0.018	0.311	0.058	-0.030	-0.065	0.462
	7	0.021	0.582	0.036	-0.039	-0.180	0.217
	9	0.024	0.949	0.022	-0.052	-0.328	0.159
	10.5	0.026	1.876	0.014	-0.062	-0.634	0.098
14.5	2	0.012	0.133	0.143	-0.022	-0.024	0.917
	4	0.019	0.327	0.037	-0.029	-0.167	0.174
	6	0.039	0.777	0.05	-0.035	-0.375	0.093
	8	0.055	1.372	0.04	-0.058	-0.655	0.089
21.6	2	0.014	0.178	0.079	-0.037	-0.057	0.649
	4	0.021	0.599	0.032	-0.06	-0.308	0.195
	6	0.032	2.156	0.015	-0.075	-0.559	0.134

water content of the weakly cemented soft rock, as shown in Fig. 6.

Figure 5 illustrates the negative exponential function relationship between the long-term strength and the water content.

Fractional order creep model

Fractional calculus theory

Fractional calculus is derived from the development of the traditional integral calculus theory, and it is able to describe the derivatives or integrals of arbitrary order (Chen et al. 2014; Liao et al. 2016). Fractional order calculus is defined in the form of an integral. The most well-known forms include the Riemann–Liouville fractional differential operator and the Caputo operator (Zhang et al. 2014).

In this case, the Riemann–Liouville definition of the calculus operator was employed, as shown in Eq. (1):

$${}^{RL}D_t^\alpha f(t) = \left(\frac{d}{dt}\right)^n I_a^{n-\alpha} f(t) = \frac{1}{\Gamma(n-\alpha)} \left(\frac{d}{dt}\right)^n \int_a^t \frac{f(\tau)d\tau}{(t-\tau)^{\alpha-n-1}}, \quad (1)$$

$(n-1 \leq \alpha < n, \quad t > a)$

The Riemann–Liouville fractional integral operator is shown in Eq. (2):

$$I_a^\alpha f(t) = \frac{1}{\Gamma(\alpha)} \int_a^t \frac{f(\tau)d\tau}{(t-\tau)^{1-\alpha}}, \quad (\alpha > 0, t > a) \quad (2)$$

where $\Gamma(\alpha)$ is the Gamma function, $\Gamma(\alpha) = \int_0^\infty t^{\alpha-1} e^{-t} dt, \text{Re}(\alpha) > 0$; D and I are differential and integral symbols, respectively; t is the upper limit of the integral; and α is the fractional order.

Fractional derivative Abel dashpot

The stress versus strain characteristics of the geotechnical materials between an ideal rigid body and an ideal fluid body can be expressed in the fractional differential form of the Abel dashpot, as shown in Fig. 7 (Zhou et al. 2011).

The stress versus strain relationship of the Abel dashpot can be calculated according to Eq. (3):

$$\sigma(t) = \xi \frac{d^\alpha \varepsilon(t)}{dt^\alpha} \quad (3)$$

where ξ is the viscosity coefficient of the Abel dashpot and α is the fractional order. Equation (3) can be reduced to Hooke’s elastic law when α is 0 and similarly to Newton’s fluid law when α is 1. The Abel dashpot can describe stress versus strain characteristics between ideal elastic and fluid materials.

The deviator stress $\sigma(t)$ was considered to have a constant value in the creep constitutive model. The creep constitutive equation of the Abel dashpot can be obtained using the Riemann–Liouville fractional differential operator theory, as shown in Eq. (4):

$$\varepsilon(t) = \frac{\sigma_0}{\xi} \frac{t^\alpha}{\Gamma(1+\alpha)} \quad (4)$$

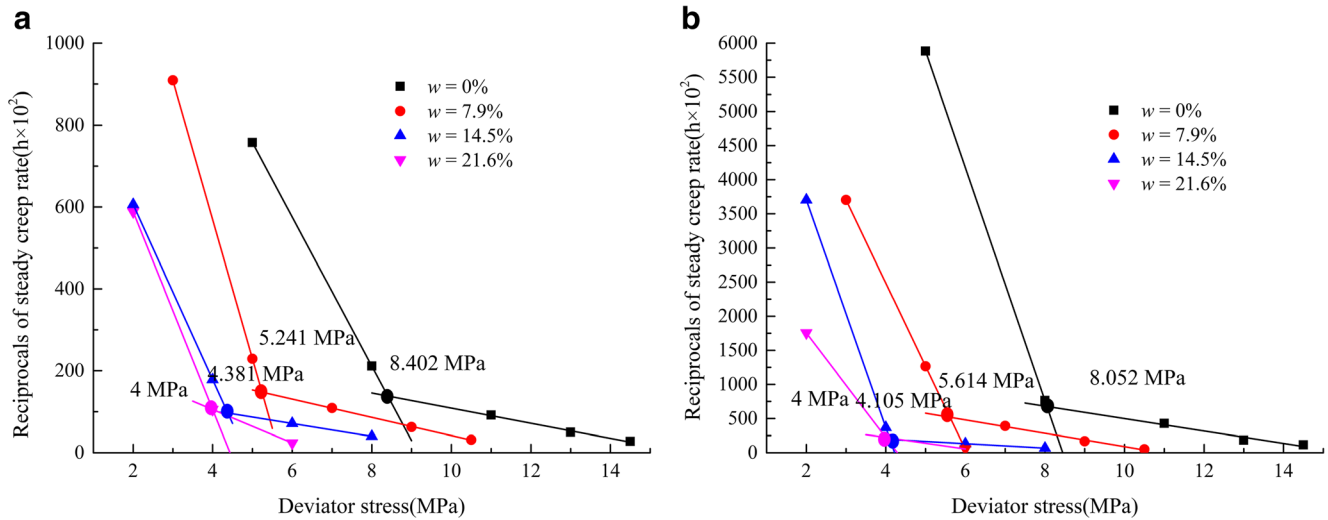


Fig. 5 Long-term strength of rock determined with the reciprocal of steady creep rate: (a) axial; (b) radial

The creep curves for different fractional orders (α) can then be obtained as shown in Fig. 8 through the dimensionless treatment of Eq. (4).

Figure 8 shows that for an α value between 0 and 1 (Fig. 8a), the stress versus strain curves gradually increase, although the growth rate slows gradually, which describes the steady-state creep characteristics of the geomaterials. In addition, the growth rate of the creep curves increases significantly when α is greater than 1 (Fig. 8b), which in turn describes the accelerated creep characteristics.

The creep rate of the Abel dashpot can be obtained from the derivation of Eq. (4), as shown in Eq. (5):

$$\dot{\varepsilon}(t) = \frac{\sigma_0}{\xi} \frac{\alpha \cdot t^{\alpha-1}}{\Gamma(1+\alpha)} dt \tag{5}$$

Equation (5) is a descending function when α is between 0 and 1, i.e., the strain rate decreases continuously during the

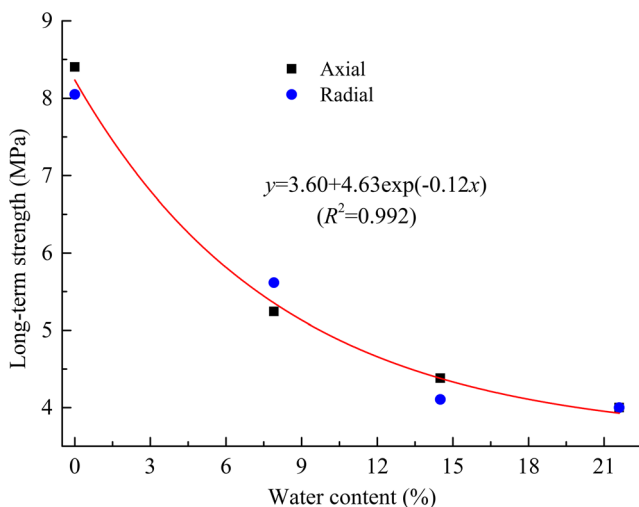


Fig. 6 Long-term strength with water content

creep process, thereby describing the attenuated creep characteristics of the rock materials. In contrast, Eq. (5) is an increasing function when α is greater than or equal to 1, which describes the accelerated creep characteristics. We can transform Eq. (5) into Eq. (6) when α is 1:

$$\dot{\varepsilon}(t) = \frac{\sigma_0}{\xi} \tag{6}$$

This equation indicates that the strain rate of Eq. (4) is constant when α is 1, thereby describing the equal velocity creep characteristics of the geomaterials.

Similarly, we assume that $\varepsilon(t)$ is a constant value (ε_0) in the stress relaxation constitutive model, and so the stress relaxation equation of the Abel dashpot is given by:

$$\sigma(t) = \xi \varepsilon_0 \frac{t^{-\alpha}}{\Gamma(1-\alpha)} \tag{7}$$

As such, the stress relaxation curves for different α values can be obtained by the dimensionless treatment of Eq. (7), as shown in Fig. 9.

As shown in Fig. 9, when α is less than 1, the stress decreases gradually over time. The reduction rate of the stress relaxation is larger in the initial stages, prior to becoming relatively stable at a later point. Thus, the relaxation is enhanced with increasing α . It is therefore evident that the Abel dashpot can clearly describe the nonlinear relaxation process of the geomaterials.

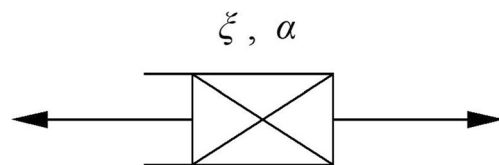


Fig. 7 Abel dashpot

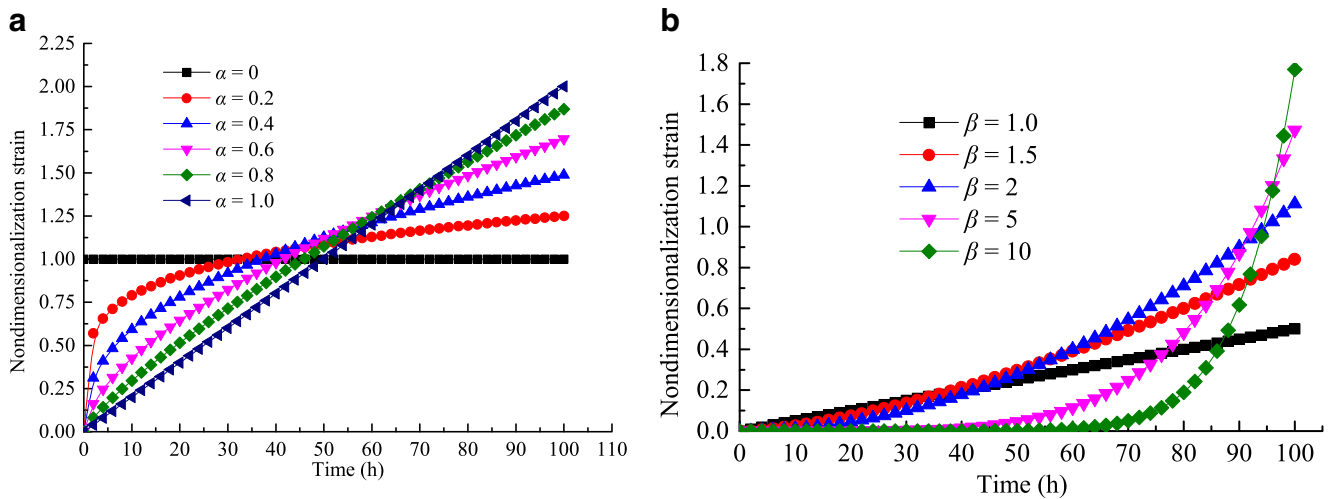


Fig. 8 Creep strain curves of Abel dashpot. (a) $\alpha \leq 1$; (b) $\alpha > 1$

Fractional-order creep model

The creep theory of soft rock has been thoroughly studied with common creep models including the Burgers model, Bingham model, and Nishihara model, the latter of which is widely used in the creep model research of geomaterials (see Fig. 10).

The creep formula of the Nishihara model can be defined according to Eqs. (8, 9) and (10):

$$\varepsilon(t) = \frac{\sigma}{E_0} + \frac{\sigma}{E_1} \left(1 - e^{-\frac{E_1 t}{\eta_1}}\right) \quad (\sigma < \sigma_s) \tag{8}$$

$$\varepsilon(t) = \frac{\sigma}{E_0} + \frac{\sigma}{E_1} \left(1 - e^{-\frac{E_1 t}{\eta_1}}\right) + \frac{\sigma - \sigma_s}{\eta_2} t \quad (\sigma \geq \sigma_s) \tag{9}$$

where E_0 and E_1 are the elastic moduli of the Hooke body, η_1 and η_2 are the viscosity coefficients of the Newton body, and σ_s is the stress threshold for accelerated creep.

According to Fig. 10 and Eqs. (8) and (9), the Nishihara model can be used to describe the instantaneous elastic strain, stress relaxation, constant-rate creep, and residual elasticity.

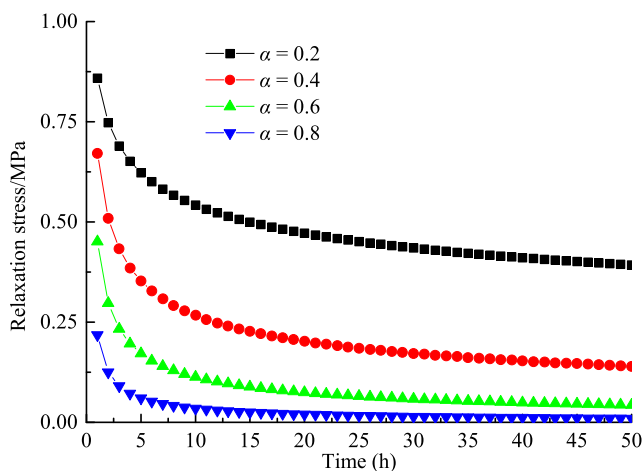


Fig. 9 Stress relaxation curves

However, it is unable to describe the accelerated creep properties of soft rock accurately. So many studies have increasingly focused on improving the creep constitutive model (Cao et al. 2002; Tomanovic 2006; Xu and Chen 2013).

Fractional calculus theory has been increasingly applied in studies of the constitutive modeling of geomaterials. Thus, we herein proposed a four-element fractional-order constitutive model of WCSR based on fractional calculus theory and the Abel dashpot, as shown in Fig. 11.

In addition, the Hooke body was employed to describe the instantaneous deformation of soft rock, while the Abel dashpot was used to describe the stress versus strain characteristics between ideal elastic and ideal fluid geomaterials ($\alpha_1 \leq 1$). In addition, the Abel dashpot, which is parallel to the plastic body, was used to characterize the accelerated creep characteristics of soft rock when the deviator stress exceeded the stress threshold ($\alpha_2 > 1$).

Thus, the fractional-order creep constitutive model of the four elements (see Fig. 10) can be deduced as follows according to the series and parallel rules of the element model. In Eq. (10), σ_0 is the deviator stress and ε_1 is the strain of the Hooke body.

$$\varepsilon_1 = \frac{\sigma_0}{E_1} \tag{10}$$

In addition, ε_2 is the strain of the Abel dashpot, and can be expressed as follows:

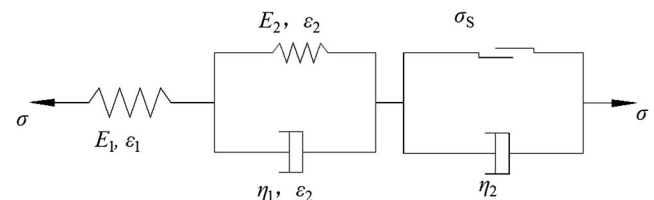


Fig. 10 Nishihara model

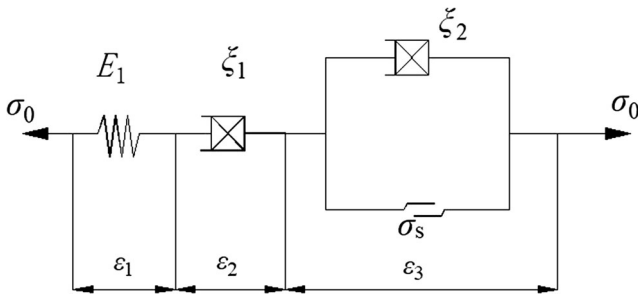


Fig. 11 Modified fractional-order model

$$\frac{d^{\alpha_1} \varepsilon_2(t)}{dt^{\alpha_1}} = \frac{\sigma_0}{\xi_1} \tag{11}$$

Furthermore, σ_3 and ε_3 are the stress and strain of the parallel combined model of the plastic element and Abel dashpot. The constitutive model can therefore be represented by Eq. (12):

$$\begin{cases} \varepsilon_3 = 0 & \sigma_0 < \sigma_s \\ \frac{d^{\alpha_2} \varepsilon_3(t)}{dt^{\alpha_2}} = \frac{\sigma_0 - \sigma_s}{\xi_2} & \sigma_0 \geq \sigma_s \end{cases} \tag{12}$$

where ξ_1 and ξ_2 are the viscosity coefficients of the attenuation and accelerated creep of the Abel dashpot, and α_1 and α_2 are the fractional orders of the creep model, where $\alpha_1 \leq 1$ and $\alpha_2 > 1$.

Assuming that the α_2 -order derivative exists for a continuous function $f(t)$, Riemann–Liouville fractional calculus can satisfy the following properties:

$${}^{RL}D_{\alpha}[f(t) + g(t)] = {}^{RL}D_{\alpha}f(t) + {}^{RL}D_{\alpha}g(t) \tag{13}$$

The combined model formula can therefore be expressed as follows:

$${}^{RL}D_{\alpha}^{\alpha_1} \varepsilon(t) = {}^{RL}D_{\alpha}^{\alpha_1} \varepsilon_1(t) + {}^{RL}D_{\alpha}^{\alpha_1} \varepsilon_2(t) \quad (\alpha_1 \leq 1 \text{ for } \sigma_0 < \sigma_s) \tag{14}$$

$${}^{RL}D_{\alpha}^{\alpha_2} \varepsilon(t) = {}^{RL}D_{\alpha}^{\alpha_1} \varepsilon_1(t) + {}^{RL}D_{\alpha}^{\alpha_1} \varepsilon_2(t) + {}^{RL}D_{\alpha}^{\alpha_2} \varepsilon_3(t) \quad (\alpha_1 \leq 1, \alpha_2 > 1 \text{ for } \sigma_0 \geq \sigma_s) \tag{15}$$

According to Eqs. (10), (11), and (14), we can deduce the following:

$${}^{RL}D_{\alpha}^{\alpha_1} \varepsilon_1(t) = \frac{1}{E_1} \frac{d^{\alpha_1} \sigma(t)}{dt^{\alpha_1}} \tag{16}$$

$${}^{RL}D_{\alpha}^{\alpha_1} \varepsilon_1(t) = \frac{1}{E_1} \frac{d^{\alpha_1} \sigma(t)}{dt^{\alpha_1}} \tag{17}$$

Assuming that the fractional derivative function ${}^{RL}D_t^{\lambda-\beta} f(t)$ exists, it has the following properties:

$${}^{RL}D_{\alpha}^{\lambda} {}^{RL}D_{\alpha}^{-\beta} f(t) = {}^{RL}D_{\alpha}^{\lambda-\beta} f(t) \quad (\lambda > 0, \beta > 0) \tag{18}$$

In particular, when $\lambda = \alpha$, we have

$${}^{RL}D_{\alpha}^{\lambda} {}^{RL}D_{\alpha}^{-\lambda} f(t) = {}^{RL}D_{\alpha}^0 f(t) - f(t) \tag{19}$$

So,

$${}^{RL}D_{\alpha}^{\alpha_2} \varepsilon_2(t) = \frac{d^{(\alpha_2+\alpha_1)} \left(\frac{\sigma(t)}{\xi_1} \right)}{dt^{(\alpha_2+\alpha_1)}} \tag{20}$$

$${}^{RL}D_{\alpha}^{\alpha_2} \varepsilon_3(t) = \frac{d^{\alpha_2} \varepsilon_3(t)}{dt^{\alpha_2}} = \frac{\sigma(t) - \sigma_s}{\xi_2} \tag{21}$$

Thus:

$${}^{RL}D_{\alpha}^{\alpha_2} \varepsilon(t) = \frac{1}{E_1} {}^{RL}D_{\alpha}^{\alpha_2} \sigma(t) + \frac{1}{\xi_1} {}^{RL}D_{\alpha}^{(\alpha_2+\alpha_1)} \sigma(t) \quad (\alpha_1 \leq 1) \text{ for } \sigma_0 \leq \sigma_s \tag{22}$$

$$\begin{aligned} {}^{RL}D_{\alpha}^{\alpha_2} \varepsilon(t) = & \frac{1}{E_1} {}^{RL}D_{\alpha}^{\alpha_2} \sigma(t) + \frac{1}{\xi_1} {}^{RL}D_{\alpha}^{(\alpha_2+\alpha_1)} \sigma(t) \\ & + \frac{\sigma(t) - \sigma_s}{\xi_2} \quad (\alpha_1 \leq 1, \alpha_2 > 1) \text{ for } \sigma_0 \geq \sigma_s \end{aligned} \tag{23}$$

(1) Creep equation

The H-Fox function is then introduced to obtain the creep model and relaxation expression.

Assuming $\sigma(t) = \sigma_0 H(t)$, then Eq. (22) can be transformed as follows:

$$\tilde{D}_t^{\alpha_1} \varepsilon = \frac{\sigma_0}{E_1} {}^{RL}D_{\alpha}^{\alpha_1} \tilde{H}(t) + \frac{\sigma_0}{\xi_1} {}^{RL}D_{\alpha}^{\alpha_1} \tilde{H}(t) \quad (\alpha_1 \leq 1) \text{ for } \sigma_0 < \sigma_s \tag{24}$$

$$\begin{aligned} \tilde{D}_t^{\alpha_2} \varepsilon = & \frac{\sigma_0}{E_1} {}^{RL}D_{\alpha}^{\alpha_2} \tilde{H}(t) + \frac{\sigma_0}{\xi_1} {}^{RL}D_{\alpha}^{(\alpha_2+\alpha_1)} \tilde{H}(t) \\ & + \frac{\sigma_0 \tilde{H}(t) - \sigma_s}{\xi_2} \quad (\alpha_1 \leq 1, \alpha_2 > 1) \text{ for } \sigma_0 \geq \sigma_s \end{aligned} \tag{25}$$

Taking Eqs. (24, 25) for the fractional Laplace transform:

$$s^{\alpha_1} = \frac{\sigma_0}{E_1} s^{\alpha_1-1} + \frac{\sigma_0}{\xi_1} s^{\alpha_1} \tag{26}$$

$$s^{\alpha_2} = \frac{\sigma_0}{E_1} s^{\alpha_2-1} + \frac{\sigma_0}{\xi_1} s^{\alpha_2+\alpha_1-1} + \frac{\sigma_0 - s\sigma_s}{s\xi_2} \tag{27}$$

Subsequently, taking the inverse Laplace transform of Eqs. (26) and (27), the four-element fractional order model can be expressed as follows:

$$\begin{aligned} \varepsilon(t) = & \frac{\sigma_0}{E_1} + \frac{\sigma_0 t^{\alpha_1}}{\xi_1} {}_{H_{1,2}}^{1,1} \left[\frac{1}{\Gamma(1+\alpha_1)} t^{\alpha_1} \Big|_{[0,1]}^{[0,1]} \quad (\alpha, \alpha) \right] \\ & (\alpha_1 \leq 1) \text{ for } \sigma_0 < \sigma_s \text{ for } \sigma_0 < \sigma_s \end{aligned} \tag{28}$$

$$\begin{aligned} \varepsilon(t) &= \frac{\sigma_0}{E_1} + \frac{\sigma_0 t^{\alpha_1}}{\xi_1} H_{1,2}^{1,1} \left[\frac{1}{\Gamma(1 + \alpha_1)} t^{\alpha_1} \middle| \begin{matrix} [0, 1] \\ [0, 1] \end{matrix} \right] (\alpha, \alpha) \\ &+ \frac{[\sigma_0 - \sigma_s] t^{\alpha_2}}{\xi_2} H_{1,2}^{1,1} \left[\frac{1}{\Gamma(1 + \alpha_2)} t^{\alpha_2} \middle| \begin{matrix} (0, 1) \\ (0, 1) \end{matrix} \right] (\alpha, \alpha) \\ &(\alpha_1 \leq 1, \alpha_2 > 1) \text{ for } \sigma_0 \geq \sigma_s \end{aligned} \tag{29}$$

where the special function is defined by the Mellin–Barnes integral as follows:

$$\begin{aligned} H_{p,q}^{m,n} \left[z \middle| \begin{matrix} (a_1, \alpha_1) \cdots (a_p, \alpha_p) \\ (b_1, \alpha_1) \cdots (b_q, \alpha_q) \end{matrix} \right] \\ = \frac{1}{2\pi i} \int \frac{\prod_{j=1}^n \Gamma(1 - a_j + a_j s) \prod_{j=1}^m \Gamma(b_j - \beta_j s)}{\prod_{j=m+1}^q \Gamma(1 - b_j + \beta_j s) \prod_{j=1}^p \Gamma(\alpha_j - \alpha_j s)} z^s ds \end{aligned} \tag{30}$$

(2) Relaxation equation

Assuming $\varepsilon = \varepsilon_0 H(t)$, then Eq. (22) can be transformed as follows:

$$\tilde{D}_t^{\alpha_2} \varepsilon_0 H(t) = \frac{1}{E_1} {}^{RL} D_t^{\alpha_2} \sigma + \frac{1}{\xi_1} {}^{RL} D_t^{(\alpha_2 + \alpha_1)} \sigma \tag{31}$$

Taking the Laplace transform of Eq. (31), we obtain:

$$s^{\alpha_2 - 1} = \tilde{\sigma} \left(\frac{1}{E_1} s^{\alpha_2} + \frac{1}{\xi_1} s^{\alpha_2 + \alpha_1} \right) \tag{32}$$

The creep equation, H-fox special function, and Laplace inverse transform were used to obtain the relaxation functions as follows:

$$\begin{aligned} \sigma(t) &= \frac{E_1 \xi_1 t^{-\alpha_1}}{E_1 + \xi_1} H_{1,2}^{1,1} \left[\frac{1}{\Gamma(1 - \alpha_1)} t^{-\alpha_1} \middle| \begin{matrix} [0, 1] \\ [0, 1] \end{matrix} \right] (-\alpha, \alpha) \varepsilon_0 \\ &\alpha_1 \leq 1 \text{ for } \sigma_0 < \sigma_s \end{aligned} \tag{33}$$

$$\begin{aligned} \sigma(t) &= \sigma_s + \frac{E_1 \xi_1 t^{-\alpha_1}}{\xi_1 + \xi_2} H_{1,2}^{1,1} \left[\frac{1}{\Gamma(1 - \alpha_1)} t^{-\alpha_1} \middle| \begin{matrix} [0, 1] \\ [0, 1] \end{matrix} \right] (-\alpha, \alpha) \varepsilon_0 \\ &+ \frac{E_1 \xi_2 t^{-\alpha_2}}{\xi_1 + \xi_2} H_{1,2}^{1,1} \left[\frac{1}{\Gamma(1 - \alpha_2)} t^{-\alpha_2} \middle| \begin{matrix} [0, 1] \\ [0, 1] \end{matrix} \right] (-\alpha, \alpha) \varepsilon_0 \\ &\alpha_1 \leq 1, \alpha_2 > 1 \text{ for } \sigma_0 \geq \sigma_s \end{aligned} \tag{34}$$

Equation (33, 34) is the stress–strain relationship of the four-element fractional model under stress relaxation conditions.

The aforementioned fractional-order constitutive model can then be employed to describe the characteristics of instantaneous deformation, steady-state creep, accelerated creep, and stress relaxation of WCSR.

Parameter solution and verification of the fractional creep model

Model parameter solution

The ant colony algorithm (ACA) is a swarm intelligence algorithm with good robustness that characterizes positive feedback and allows for a parallel search. The parameters of the four-element fractional creep constitutive model are regarded as a group of optimization problems. Therefore, the ant colony optimization algorithm is employed to search the optimal objective function value to obtain the appropriate combination parameter values.

The specific algorithm steps are shown in Fig. 12 (Yao et al. 2016; Zhuang et al. 2011).

In Fig. 12, $X = \{E_1, \xi_1, \alpha_1, \xi_2, \alpha_2\}$ are the creep model parameters that are randomly assigned to each ant. Range of parameters are $E_1 \in [0, 1000]$, $\xi_1 \in [0, 200]$, $\xi_2 \in [10^3, 10^6]$, $\alpha_1 \in [0, 1]$, and $\alpha_2 \in [1, 20]$. $\Delta t(i)$ is the error of the creep model, β is the basic parameter, and $\beta = 3$. “Error” represents the error index function, where $Error(i) = [\varepsilon_j^*(i) - \varepsilon_t(i)]^2$ and $\varepsilon_j^*(i)$ is the calculated value of the deformation using the creep model equations, Eqs. (28) and (29). $\varepsilon_t(i)$ is the test results. “BIndex” is the ant with the largest pheromone, δ is the pheromone volatilization factor, $K = 0.1$. “Echo” represents the current evolutionary algebra of the ant colony, and “Echo_{max}” represents the largest evolutionary algebra of the ant colony, where Echo_{max} is 100.

We assume the ant number (m) is 30 and calculate $e^{-T_0(i)}$, $i = 1, 2, \dots, m$. The calculated results are arranged in ascending order as $T_1(j)$, where $j = 1, 2, \dots, m$. The dynamic transfer factor can be calculated as Eq. (35).

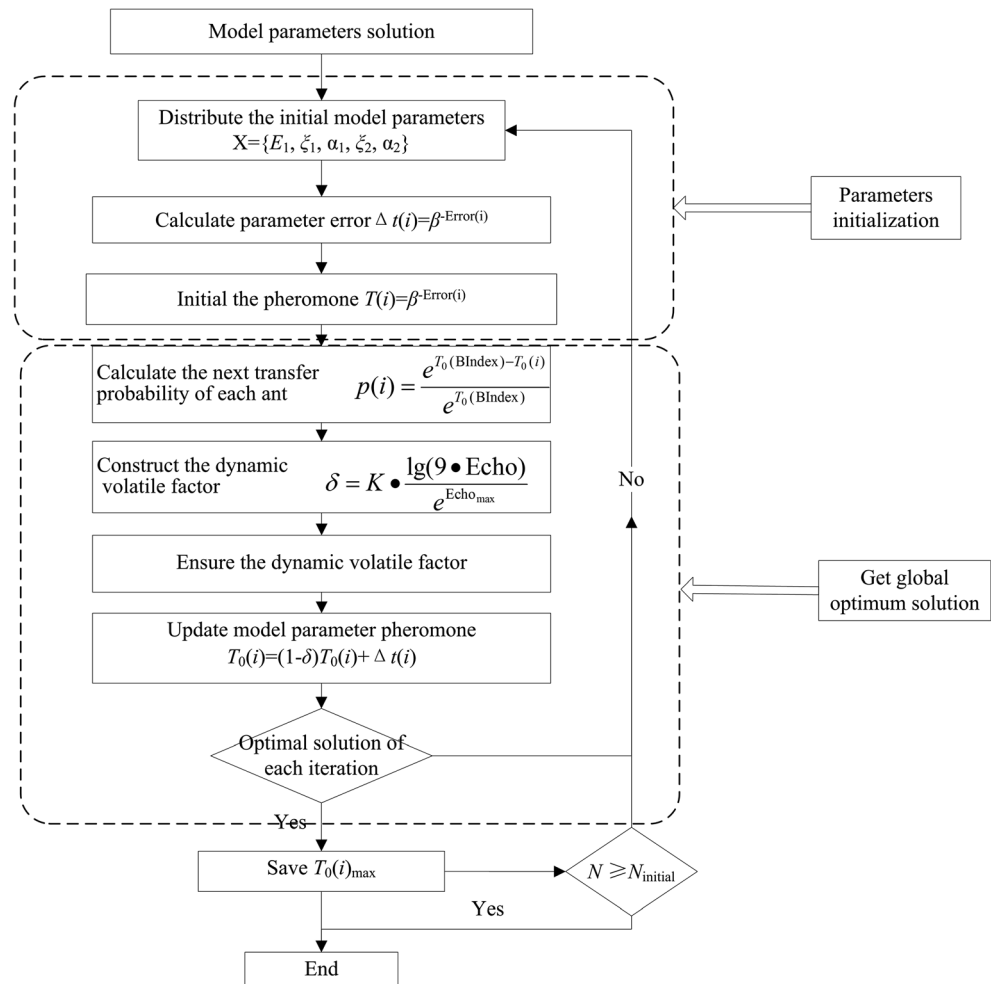
$$\begin{cases} p_0 = t_1 \left(\frac{2}{3} m \right), & Echo < \left(\frac{Echo_{max}}{2} \right) \\ p_0 = t_1 \left(\frac{1}{2} m \right), & else \end{cases} \tag{35}$$

A local search is performed if $p(i) < p_0$, otherwise a global search is performed. In this way, a better solution will obtain at the beginning, and the search will avoid falling into a local optimum during the search process.

Then, the pheromone of the creep model parameters is update and the largest pheromone is saved. The error value is calculated according to the error model. Then the process returns to the parameter initialization to carry out the iteration cycle. The search ends when the number of iterations reaches the initial setting. The optimization creep model parameters are obtained from the best ants.

The parameters of the Nishihara model and four-element fractional creep constitutive model were obtained by using the above method, as shown in Tables 3 and 4.

Fig. 12 The flow chart of procedure of ACA



Model verification

Substituting the aforementioned model parameters into Eqs. (28) and (29), the calculated values of the model could be compared with the experimental results, as shown in Fig. 13.

As shown in Fig. 13, the tests were performed in the stable creep stage, and the Nishihara model and four-element fractional-order creep model give higher values than those obtained in the tests. In addition, the correlation coefficients are satisfactory (i.e., $R^2 \geq 0.85$); however, a higher value was obtained for the fractional creep model correlation coefficient (i.e., $R^2 \geq 0.93$). As such, both models can reasonably describe the steady-state creep characteristics of WCSR. However, the Nishihara model cannot describe the accelerated creep characteristics of the specimen, as a large error was obtained in this case (correlation coefficient $R^2 \geq 0.93$). Moreover, the calculation results obtained using this model suggests a trend of constant velocity growth, which is inconsistent with the trend of an accelerated creep rate increase. We also found that the four-element fractional creep model can reasonably describe the instantaneous deformation, decay rheology, constant velocity rheology, and accelerated rheology of WCSR, in

particular when describing the accelerated creep curves with $R^2 = 0.924\text{--}0.991$. These results therefore indicate that the four-element fractional creep model proposed herein can reasonably reflect the creep variation of weakly cemented soft rock.

Conclusions

In this study, a series of triaxial creep tests were performed to study the creep properties of weakly cemented soft rock. Then, a four-element fractional creep constitutive model was established basing on the fractional calculus theory. The main conclusions are as follows:

1. Test results show that moisture content and deviator stress have significant influence on creep behavior of weakly cemented soft rock. The creep curves gradually change from two-stage steady-state creep to three-stage unsteady-state creep and accelerated creep occurs, eventually. The instantaneous deformation, creep deformation, axial initial creep rate, and steady creep rate increase with the water content and

Table 3 Parameters of Nishihara’s model

Samples	w (%)	σ_0 (MPa)	Axial strain					Radial strain				
			E_1 (MPa)	E_2 (MPa)	η_1 (MPa·h)	η_2 (MPa·h)	R^2	E_1 (MPa)	E_2 (MPa)	η_1 (MPa·h)	η_2 (MPa·h)	R^2
R11	0	5	118.6	83.98	929.9		0.934	559.6	486.1	1267		0.885
R12		8	174.8	42.28	388.4		0.985	488.5	246.7	1691		0.989
R13		11	167.9	21.38	539.7		0.995	433.7	176.8	4408		0.984
R14		13	150.1	14.40	318.1		0.995	327.4	64.0	3312		0.992
R15		14.5	121.6	43.08	128.1	27.76	0.967	501.6	322.5	4524	248.5	0.765
R21	7.9	3	68.4	39.65	377.7		0.944	285	259.4	825.6		0.852
R22		5	152.7	17.32	204.3		0.994	262.5	181.8	1048		0.990
R23		7	100.3	12.27	288.3		0.986	197.3	92.14	2003		0.972
R24		9	156.2	9.36	193.3		0.995	207.2	34.01	2148		0.938
R25		10.5	133.2	25.88	50.0	27.39	0.961	357.4	277.8	271.9	189.2	0.778
R31	14.5	2	35.9	23.89	227.7		0.928	181.5	172.0	854		0.992
R32		4	71.7	14.46	216.7		0.984	150.7	48.13	1465		0.980
R33		6	45.2	7.96	201.2		0.991	138.5	22.37	1236		0.990
R34		8	166.5	41.58	18.85	40.68	0.936	266.4	341.6	1325	175.2	0.807
R41	21.6	2	24.3	20.51	181.9		0.865	64.55	154.7	104.0		0.892
R42		4	28.7	8.95	106.2		0.962	84.46	20.6	363.1		0.986
R43		6	41.5	17.96	18.2	29.67	0.954	160.9	325.6	906.1	190	0.882

deviator stress increase, while the influence of water content on the radial initial creep rate curves is not consistent.

2. The total deformation increases with the water content and deviator stress increase. And the ratio of the creep

deformation to instantaneous deformation also increases, which indicates that the WCSR with water content perform obvious creep characteristics under the action of long-term load. The long-term strength of weakly cemented soft rock

Table 4 Parameters of four-element fractional-order model

Samples	w (%)	σ_0 (MPa)	Axial strain					Radial strain						
			E_1 (MPa)	α_1	ξ_1 (MPa·h $^{\alpha_1}$)	α_2	ξ_2 (GPa·h $^{\alpha_2}$)	R^2	E_1 (MPa)	α_1	ξ_1 (MPa·h $^{\alpha_1}$)	α_2	ξ_2 (GPa·h $^{\alpha_2}$)	R^2
R11	0	5	530.1	0.232	138.9			0.990	552.9	0.088	683.2			0.948
R12		8	819.5	0.300	110.2			0.972	964.9	0.229	485.3			0.939
R13		11	207.2	0.502	167.9			0.998	625.2	0.488	130.7			0.998
R14		13	976.8	0.508	112.2			0.997	477.4	0.634	124.0			0.998
R15		14.5	1290	0.624	131.6	10.28	5×10^5	0.974	742.9	0.214	297	6.127	1.2×10^4	0.924
R21	7.9	3	576.6	0.230	65.68			0.987	298	0.084	339.1			0.949
R22		5	575.3	0.393	73.86			0.968	454.3	0.160	261.6			0.985
R23		7	680.4	0.488	88.83			0.996	424.5	0.379	385.0			0.995
R24		9	759.7	0.533	80.95			0.993	274.5	0.692	948.3			0.998
R25		10.5	801.0	0.529	59.81	8.758	1×10^5	0.978	621.2	0.242	198.4	6.236	1.13×10^4	0.954
R31	14.5	2	201.4	0.223	37.6			0.985	182.1	0.026	189.1			0.990
R32		4	520.8	0.378	56.76			0.991	298.3	0.477	356.6			0.995
R33		6	174.5	0.487	58.47			0.998	222.6	0.638	457.1			0.999
R34		8	214.5	0.368	41.72	5.739	0.8×10^5	0.999	477.6	0.284	158.7	6.567	1.02×10^4	0.977
R41	21.6	2	298.1	0.179	23.63			0.971	105	0.145	141.9			0.949
R42		4	129.7	0.27	20.73			0.979	131.4	0.581	289.2			0.995
R43		6	100.5	0.531	27.98	10.31	1.0×10^5	0.996	186	0.326	142	4.929	0.79×10^4	0.991

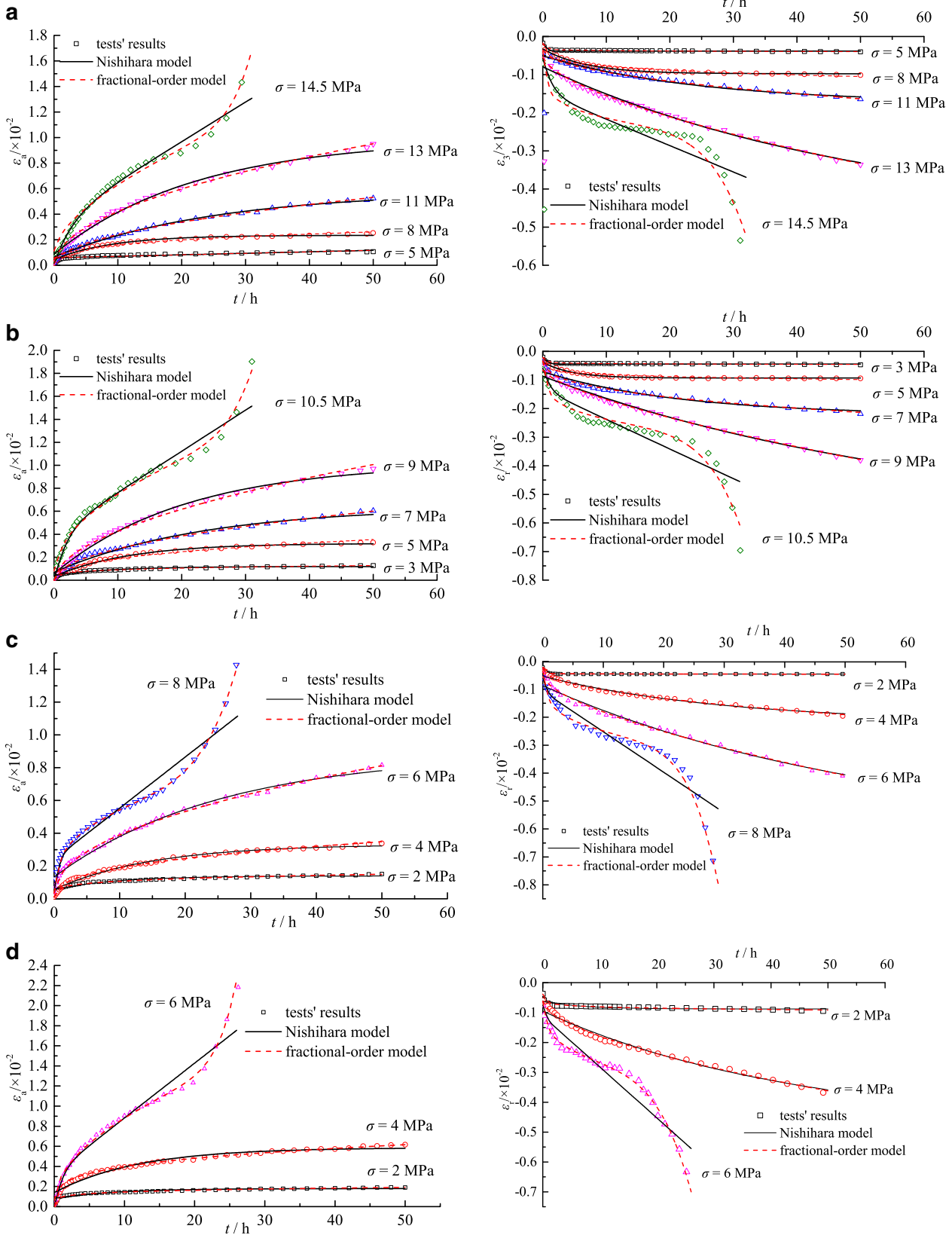


Fig. 13 Test and model verification results. (a) $w = 0\%$; (b) $w = 7.9\%$; (c) $w = 14.5\%$; (d) $w = 21.6\%$

was obtained by using the reciprocal of steady creep rate method. The long-term strength decreases with the increase of water content and the relationship between long-term strength and water content shows a good negative exponential function.

3. A four-element fractional creep constitutive model of weakly cement soft rock was proposed basing on fractional calculus theory. The specific creep equation and relaxation equation of the model were obtained by introducing the H-Fox special function. The constructed model can describe the steady creep, unsteady creep, and stress relaxation of soft rock. In addition, it only contains only five parameters, which could be easily acquired.

4. The model parameters were obtained by trust-region method and optimized by the ant colony optimization algorithm method. The parameters were taken into the four-element fractional creep constitutive model to calculate the creep deformation with different water and deviator stress conditions. Comparison results show that the four-element fractional creep constitutive model can accurately simulate the steady and unsteady creep characteristics of weakly cemented soft rock, especially for accelerated creep behavior.

These research results will be helpful for studying the stability of weakly cemented soft rock mine engineering.

Acknowledgments This work was supported by the State Key Laboratory for Geomechanics and Deep Underground Engineering, China University of Mining & Technology (grant no. SKLGDUEK1914), the State Key Program of National Natural Science of China (grant no. 51734009), the National Natural Science Foundation of China (grant no. 51704144), and Liaoning Natural Science Foundation Guidance Project (grant no. 20180551162). The authors gratefully acknowledge the helpful comments made by the reviewers.

References

- Ajalloeian R, Lashkaripour GR (2000) Strength anisotropies in mudrock. *Bull Eng Geol Environ* 59:195–199. <https://doi.org/10.1007/s100640000055>
- Arikoglu A (2014) A new fractional derivative model for linearly viscoelastic materials and parameter identification via genetic algorithms. *Rheol Acta* 53:219–233. <https://doi.org/10.1007/s00397-014-0758-2>
- Bouras Y, Zorica D, Atanacković TM, Vrcelj Z (2018) A non-linear thermo-viscoelastic creep model based on fractional derivatives for high temperature creep in concrete. *Appl Math Model* 55:551–568. <https://doi.org/10.1016/j.apm.2017.11.028>
- Cao S, Bian J, Li P (2002) Rheologic constitutive relationship of rock and a modified model. *Chin J Rock Mech Eng* 21:632–634. <https://doi.org/10.3321/j.issn:1000-6915.2002.05.004>
- Chen BR, Zhao XJ, Feng XT, Zhao HB, Wang SY (2014) Time-dependent damage constitutive model for the marble in the Jinping II hydropower station in China. *Bull Eng Geol Environ* 73:499–515. <https://doi.org/10.1007/s10064-013-0542-z>
- Chen JR, Pu H, Xiao C (2015) Research on rheology model of broken mudstone based on the fractional theory. *J China Univ Min Technol* 44:996–1001. <https://doi.org/10.13247/j.cnki.jcumt.000418>
- Chenevert EM (1970) Shale alteration by water adsorption. *J Pet Technol* 22:1141–1148. <https://doi.org/10.2118/2401-pa>
- Deng HF, Zhou ML, Li JL, Sun XS, Huang YL (2016) Creep degradation mechanism by water–rock interaction in the red-layer soft rock. *Arab J Geosci* 9:601. <https://doi.org/10.1007/s12517-016-2604-6>
- Duan XM, Yin DS, An LY, Zhang W (2013) The deformation study in viscoelastic materials based on fractional order calculus. *Sci Sin Phys Mech Astron* 43:971. <https://doi.org/10.1360/132012-807>
- Feng WL, Qiao CS, Niu SJ (2020) Study on sandstone creep properties of Jushan Mine affected by degree of damage and confining pressure. *Bull Eng Geol Environ* 79(2):869–888. <https://doi.org/10.1007/s10064-019-01615-x>
- Heymans N, Bauwens JC (1994) Fractal creep models and fractional differential equations for viscoelastic behavior. *Rheol Acta* 33: 210–219. <https://doi.org/10.1007/BF00437306>
- Hong Z, Xia-Ting F, Xian-jie H (2015) A creep model for weakly consolidated porous sandstone including volumetric creep. *Int J Rock Mech Min Sci* 78:99–107. <https://doi.org/10.1016/j.ijrmmms.2015.04.021>
- Hou RB, Zhang K, Tao J, Xue XR, Chen YL (2019) A nonlinear creep damage coupled model for rock considering the effect of initial damage. *Rock Mech Rock Eng*:1275–1285. <https://doi.org/10.1007/s00603-018-1626-7>
- Huang M, Liu XR (2011) Study on the relationship between parameters of deterioration creep model of rock under different modeling assumptions. *Adv Mater Res* 243–249:2571–2580. <https://doi.org/10.4028/www.scientific.net/AMR.243-249.2571>
- Jiang HF, Liu DY, Huang W et al. (2014) Creep properties of rock under high confining pressure and different pore water pressures and a modified Nishihara model. *Chin J Geotech Eng* 36(3):443–451. <https://doi.org/10.11779/CJGE201403006>
- Işık Y (2010) Influence of water content on the strength and deformability of gypsum. *Int J Rock Mech Min Sci* 47:342–347. <https://doi.org/10.1016/j.ijrmmms.2009.09.002>
- Ju N, Haifeng H, Da Z, Xin Z, Chengqiang Z (2016) Improved Burgers model for creep characteristics of red bed mudstone considering water content. *Rock Soil Mech* 67:–74. <https://doi.org/10.16285/j.rsm.2016.S2.008>
- Li P, Liu J, Zhu JB, He HJ (2008) Research on effects of water content on shear creep behavior of weak structural plane of sandstone. *Rock Soil Mech* 29:1865–1871. <https://doi.org/10.3901/JME.2008.10.294>
- Li RD, Yue JC, Zhu CZ, Sun ZY (2013) A nonlinear viscoelastic creep model of soft soil based on fractional order derivative. *Appl Mech Mater* 438–439:1056–1059. <https://doi.org/10.4028/www.scientific.net/AMM.438-439.1056>
- Li DW, Chen JH, Zhou Y (2018) A study of coupled creep damaged constitutive model of artificial frozen soil. *Adv Mater Sci Eng* 2018: 1–9. <https://doi.org/10.1155/2018/7458696>
- Liao MK, Lai YM, Liu EL, Wan XS (2016) A fractional order creep constitutive model of warm frozen silt. *Acta Geotech* 12:1–13. <https://doi.org/10.1007/s11440-016-0466-4>
- Liu X, Chao Y, Jing Y (2015) The influence of moisture content on the time-dependent characteristics of rock material and its application to the construction of a tunnel portal. *Adv Mater Sci Eng*: 1–13. <https://doi.org/10.1155/2015/725162>
- Liu HZ, Xie HQ, He JD, Xiao ML, Zhuo L (2016) Nonlinear creep damage constitutive model for soft rock. *Mech Time Dependent Mater* 21:1–24. <https://doi.org/10.1007/s11043-016-9319-7>
- Matthess G (1988) Advances in modelling water-rock interaction in aquifers[M]// groundwater flow and quality modelling. Springer Netherlands. https://doi.org/10.1007/978-94-009-2889-3_23
- Metzler R, Nonnenmacher TF (2003) Fractional relaxation processes and fractional creep models for the description of a class of viscoelastic materials. *Int J Plast* 19:941–959. [https://doi.org/10.1016/s0749-6419\(02\)00087-6](https://doi.org/10.1016/s0749-6419(02)00087-6)

- Ofoegbu GI, Dasgupta B, Manepally C, Stothoff SA, Fedors R (2017) Modeling the mechanical behavior of unsaturated expansive soils based on bishop principle of effective stress. *Environ Earth Sci* 76: 555. <https://doi.org/10.1007/s12665-017-6884-2>
- Papoulia KD, Panoskaltis VP, Kurup NV, Korovajchuk I (2010) Creep representation of fractional order viscoelastic material models. *Rheol Acta* 49:381–400. <https://doi.org/10.1007/s00397-010-0436-y>
- Pu SY, Huang ZH, Yao JY, Mu R, Zheng HC, Wang TL, Liu XL, Li L, Wang YH (2018) Fractional-order Burgers constitutive model for rock under low dynamic stress. *J Yangtze River Sci Res Inst*. <https://doi.org/10.11988/ckyyb.20170454>
- Roedder E, Bassett RL (1981) Problems in determination of the water content of rock-salt samples and its significance in nuclear-waste storage siting. *Geol* 9(11):92–104. [https://doi.org/10.1130/0091-7613\(1981\)92.0.CO;2](https://doi.org/10.1130/0091-7613(1981)92.0.CO;2)
- Shi X, Cai W, Meng Y, Li G, Wen K, Zhang Y (2016) Weakening laws of rock uniaxial compressive strength with consideration of water content and rock porosity. *Arab J Geosci* 9:1–7. <https://doi.org/10.1007/s12517-016-2426-6>
- Su T, Zhou HW, Zhao JW, Che J, Sun XT, Wang L (2019) A creep model of rock based on variable order fractional derivative. *Chin J Rock Mech Eng* 38(7):1355–1363. <https://doi.org/10.13722/j.cnki.jrme.2018.1382>
- Sun J, Wang S (2000) Rock mechanics and rock engineering in China: developments and current state-of-the-art. 37:447–465. [https://doi.org/10.1016/S1365-1609\(99\)00072-6](https://doi.org/10.1016/S1365-1609(99)00072-6)
- Tang H, Wang DP, Huang RQ, Pei XJ, Chen WL (2017) A new rock creep model based on variable-order fractional derivatives and continuum damage mechanics. *Bull Eng Geol Environ*:1–9. <https://doi.org/10.1007/s10064-016-0992-1>
- Tang H, Duan Z, Wang DP, Dang Q (2020) Experimental investigation of creep behavior of loess under different moisture contents. *Bull Eng Geol Environ* 79(1):411–422. <https://doi.org/10.1007/s10064-019-01545-8>
- Tomanovic Z (2006) Creep model of soft rock creep based on the tests on marl mechanics of time-dependent materials. 10:135–154. <https://doi.org/10.1007/s11043-006-9005-2>
- Wang JB, Liu XR, Song ZP et al (2018) A whole process creeping model of salt rock under uniaxial compression based on inverse S function. *Chin J Rock Mech Eng* 37(11):27–40
- Wei HZ, Xu WJ, Wei CF, Meng QS (2018) Influence of water content and shear rate on the mechanical behavior of soil–rock mixtures. *Sci China Technol Sci* 61:1127–1136. <https://doi.org/10.1007/s11431-017-9277-5>
- Wu F, Xie HP, Liu JF, Bian Y, Pei JL (2014) Experimental study of fractional viscoelastic-plastic creep model. *Chin J Rock Mech Eng* 33:964–970. <https://doi.org/10.13722/j.cnki.jrme.2014.05.012>
- Wu F, Liu JF, Wang J (2015) An improved Maxwell creep model for rock based on variable-order fractional derivatives. *Environ Earth Sci* 73: 6965–6971. <https://doi.org/10.1007/s12665-015-4137-9>
- Xu Z, Chen W (2013) A fractional-order model on new experiments of linear viscoelastic creep of Hami Melon. *Comput Math Appl* 66: 677–681. <https://doi.org/10.1016/j.camwa.2013.01.033>
- Xu HY, Jiang XY (2017) Creep constitutive models for viscoelastic materials based on fractional derivatives. *Comput Math Appl* 73:1377–1384. <https://doi.org/10.1016/j.camwa.2016.05.002>
- Yang CH, Wang YY, Jian-Guang LI, Gao F (2007) Testing study about the effect of different water content on rock creep law. *J China Coal Soc* 32:695–699. <https://doi.org/10.1007/s10870-007-9222-9>
- Yao Z, Zhang Q, Niu L (2016) Analysis of fractional order derivative Nishihara model of frozen remolded clay based on ant colony algorithm. *J Yangtze River Sci Res Inst* 33:81–86. <https://doi.org/10.11988/ckyyb.20150419>
- Yuan WW (2014) Research on fractional damage model of mudstone dynamic creep. *Northeast Petroleum Univ*:29–39
- Zhang Q, Li SC, Li LP, Zhang QQ (2013) Experimental study on creep of highly-weathered breccia. *Appl Mech Mater* 477-478:588–591. <https://doi.org/10.4028/www.scientific.net/amm.477-478.588>
- Zhang Y, Xu WY, Wang W, Shao JF, Gu JJ (2014) Study of creep tests and its parameters identification of soft rock in fractured belt. *Chin J Rock Mech Eng* 33:3412–3420. <https://doi.org/10.13722/j.cnki.jrme.2014.s2.004>
- Zhou HW, Wang CP, Han BB, Duan ZQ (2011) A creep constitutive model for salt rock based on fractional derivatives. *Int J Rock Mech Min Sci* 48:116–121. <https://doi.org/10.1016/j.ijrmmms.2010.11.004>
- Zhou HW, Wang CP, Mishnaevsky L, Duan ZQ, Ding JY (2013) A fractional derivative approach to full creep regions in salt rock. *Mech Time Dependent Mater* 17:413–425. <https://doi.org/10.1007/s11043-012-9193-x7>
- Zhuang Y, Bai ZL, Xu YF (2011) Research on parameters of support vector machine based on ant colony algorithm computer simulation. 28:216–219. <https://doi.org/10.1016/j.cageo.2010.07.006>